Folding and stacking defects of graphene flakes probed by electron nanobeam

L. Persichetti, F. Tombolini, S. Casciardi, M. Diociaiuti, M. Fanfoni, G. Palleschi, A. Sgarlata, F. Valentini, and A. Balzarotti

Citation: Applied Physics Letters **99**, 041904 (2011); doi: 10.1063/1.3615802
View online: http://dx.doi.org/10.1063/1.3615802
View Table of Contents: http://scitation.aip.org/content/aip/journal/apl/99/4?ver=pdfcov
Published by the AIP Publishing

Folding and stacking defects of graphene flakes probed by electron nanobeam

L. Persichetti,[1,a)] F. Tombolini,[2] S. Casciardi,[2] M. Diociaiuti,[3] M. Fanfoni,[1] G. Palleschi,[4] A. Sgarlata,[1] F. Valentini,[4] and A. Balzarotti[1]
[1]*Dipartimento di Fisica, Università degli studi di Roma Tor Vergata, via della Ricerca Scientifica 1, 00133 Roma, Italy*
[2]*Dipartimento di Igiene del Lavoro, INAIL ex ISPESL, 00040 Monte Porzio Catone, Italy*
[3]*Dipartimento di Tecnologie e Salute, Istituto Superiore di Sanità, 00161 Roma, Italy*
[4]*Dipartimento di Scienze e Tecnologie Chimiche, Università degli studi di Roma Tor Vergata, via della Ricerca Scientifica 1, 00133 Roma, Italy*

(Received 18 May 2011; accepted 30 June 2011; published online 27 July 2011)

Combining nanoscale imaging with local electron spectroscopy and diffraction has provided direct information on folding and stacking defects of graphene flakes produced by unrolled multi-walled carbon nanotubes. Structural data obtained by nanoarea electron diffraction complemented with systematic electron energy loss spectroscopy measurements of the surface plasmon losses of single flakes show the presence of flat bilayer regions coexisting with folded areas where the topology of buckled graphene resembles that of warped carbon nanostructures. © *2011 American Institute of Physics*. [doi:10.1063/1.3615802]

Since 2004, when Novoselov, Geim, and coworkers reported a method for graphene production by the peeling of highly oriented pyrolytic graphite (HOPG),[1] the properties of this two-dimensional crystal have fascinated the scientific community, subsequently becoming the subject of intensive research.[2–4] Recently, carbon structures with sp^2 hybridization, such as bilayer, few-layer graphene, and graphene nanoribbons have entered the flat nanocarbon world.[5] Each of these systems exhibits peculiar properties which are different from both graphene and graphite.[6] In recent years, many methods have been developed to produce graphene flakes and nanoribbons, such as chemical vapor deposition and chemical or lithographic treatments of graphite (see, e.g., Refs. 5 and 7). Nowadays, the unzipping of single and multiwalled nanotubes offers a viable route for large-scale synthesis of graphene flakes.[8] However, most properties of graphene films and graphene nanoribbons remain unexplained and, therefore, cannot be controlled without a knowledge of the structural defects such as spontaneous warping of the sheets.[9–11] The tendency to warping is even larger in nanoribbons for which twisted and scrolled configurations are predicted to be energetically favored beyond a critical size.[12–14]

In this paper, we use scanning tunneling microscopy (STM) and transmission electron microscopy (TEM) to investigate folding and stacking defects of graphene flakes. The structure of the defective surface is studied by nanoarea electron diffraction (NED) and correlated with the thickness of individual flakes measured by electron energy loss spectroscopy (EELS).

Briefly, graphene sheets were prepared by unzipping Mitsui multi-wall carbon nanotubes (MWCNTs) with $KMnO_4$ (Refs. 15 and 16) and removing almost all small-molecule impurities by repeated washing with aqueous HCl, ethanol, and ether. The oxidized ribbons were then dispersed in water and 95% ethanol. The ribbons were reduced with hydrazine[17] and the reduced flakes were stored as a suspension in 200 ml aqueous solution ($pH = 10$) of hydrazine (ca. 100 μl of $N_2H_4 \bullet H_2O$) in the presence of ammonia (ca. 100 μl of NH_4OH). For TEM analysis, a drop of suspension was deposited on gold TEM grids (1000 mesh) directly from solution. High-resolution experiments were performed with a FEI TECNAI 12 G2 Twin TEM microscope operating at 120 kV and equipped with an electron energy filter (Gatan image filter), a slow-scan charge-coupled device camera (Gatan multiscan), and a x-ray energy dispersive spectrometer (EDAX Inc.). NED and EELS measurements were made using a nanometer-sized coherent parallel beam of electrons. Since the collection angle is approximately 20 mrad for EELS, the momentum $\mathbf{q}$ has a maximum in-plane component of 2.4 $Å^{-1}$ and, thus, plasmons with $\mathbf{q}$ mainly parallel to the ***a***-axis of graphene can be excited.[18] Unlike conventional selected area electron diffraction (SAED), the diffraction volume is defined directly by the electron probe in NED.[19] By reducing the size of the incident electron beam to a few nanometers with the condenser aperture and the spot size condenser lens, EELS spectra and diffraction patterns were acquired on individual ribbons. To ensure the reliability of the measurements, the area from which electrons are collected was imaged before and after exposure to the beam. STM measurements were carried out in an ultrahigh vacuum chamber (base pressure 4×10^{-11} mbar) on flakes deposited on HOPG substrates. Since graphite is lattice matched to graphene, it offers support without disturbing the graphene lattice symmetry. STM images were collected at ambient temperature using chemically etched W tips.

Both TEM and STM measurements indicate that the flakes assume rolled [Figs. 1(a) and 1(b)] as well as flat configurations [Figs. 1(c) and 1(d)]. In particular, it seems that, after a critical size of a few tens of nanometers, planar ribbons crumple up and undergo folding and twisting [See sketch in Fig. 1(a)]. According to recent simulations,[12–14]

[a)]Author to whom correspondence should be addressed. Electronic mail: persichetti@roma2.infn.it.

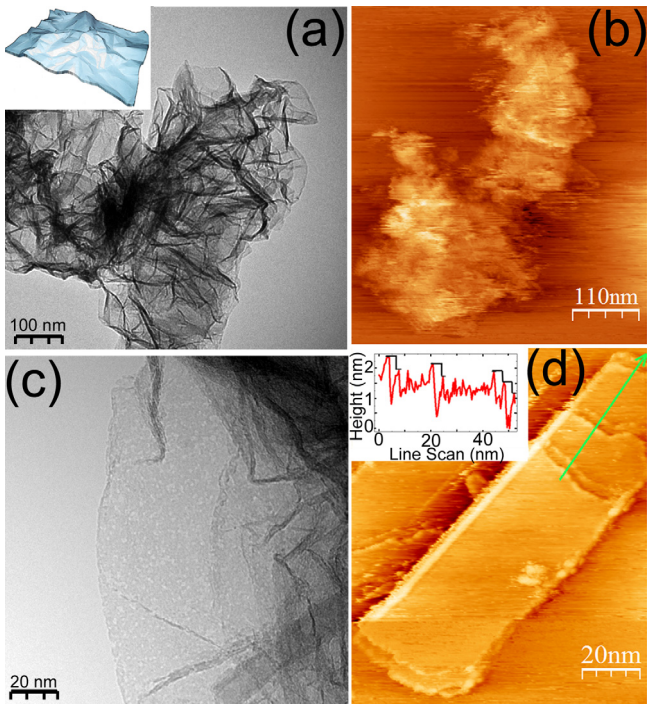

FIG. 1. (Color online) TEM and STM images of the graphene flakes obtained from the oxidative unzipping of MWCNTs. (a) and (b) Warped configurations of a flake imaged by (a) TEM and (b) STM measurements. The inset of panel (a) shows a schematic drawing of a graphene multilayer. (c) and (d) Planar regions observed by (c) TEM and (d) STM. In the inset of panel (d), the STM height profile of the graphene sheet along the arrowed line is displayed.

this experimental evidence can be explained by the energy gain due to the van der Waals interactions of the overlapping layers, this, for large ribbons, outweighing the elastic energy increase caused by bending. The images displayed in Figs. 1(c) and 1(d) clearly show the layered structure of the sheets. Moreover, the STM height profile of the nanoribbon, shown in panel (d), exhibits well-defined peaks corresponding to single graphene layers with an interlayer spacing of $d_c = (0.36 \pm 0.03)$ nm.

In Figure 2(a), we report a high resolution TEM image of a graphene flake compared to the area illuminated by the electron nanobeam [the bright area in the dark background shown in panel (b)]. The small beam size makes it possible to probe small volumes of the specimen and, hence, to observe features induced by defects with high spatial resolution. For instance, in region 1 (circled) of Fig. 2(a), the diffraction pattern shows twin six-fold symmetric spots [Fig. 2(c)], corresponding to a couple of flat layers with different stacking.[20] The inner spots correspond to (10) lattice planes and the outer spots to (11) planes.[9] The spot separation, reported in Table I, indicates the good crystalline structure of the layers. In region 2 of Fig. 2(a) in which extensive folding of sheets is present, the diffraction pattern is markedly changed. Here, the ***c***-axis is locally tilted from the incident beam direction and the sequence of layers along the ***c***-axis is imaged. The sheet periodicity induces two closely spaced peaks in Fig. 2(d) from which an interlayer spacing, d_c, is estimated, resulting in a good match with STM data (Table I). Moreover, Debye rings due to the lack of crystallographic orientation among the sheets are also present. Depending on the degree of folding, some diffraction patterns have intermediate features between those of Figs. 2(c) and 2(d). An example is given in Fig. 2(e) in which the six-fold symmetry of (10) and (11) spots indicates a higher degree of ordering than panel (d). We stress that the observed changes are completely averaged out using conventional SAED, due to the lack of spatial resolution. Since the thinnest flakes are just a few tens of nanometers wide, the beam intensity in SAED is too low to record a diffraction pattern from them (see supplementary material for comparison[26]).

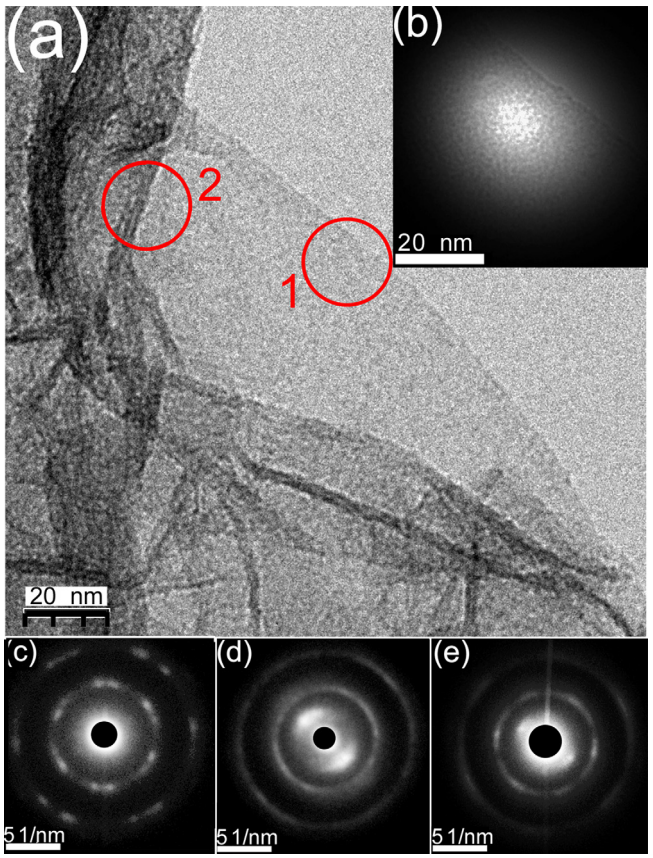

FIG. 2. (Color online) (a) High-resolution TEM image a graphene flake compared to the area illuminated by the electron nanobeam shown in panel (b). (c)-(e) NED patterns of different regions of the flakes. Panel (c) is recorded from the area labeled as 1 in panel (a), while panel (d) from the region 2. Panel (e) corresponds to an area of the sample (not shown) having intermediate folding.

The deviation from the ideal structure changes the relative direction of π and σ carbon orbitals and results into modified surface electronic properties, closely resembling

TABLE I. Energy position of the plasmon losses and structural parameters of graphene flakes of increasing thickness obtained using NED-EELS. The uncertainty about the values of the plasmon losses estimated from the full-half-width-maximum of the elastic peak is ± 0.6 eV. d_{hk}, d_c, and t_r are the lattice plane separations, the interlayer spacing and the relative thickness of the samples, respectively. A parallel electron beam having a size of ~20 nm is employed.

Sample	E_π (eV)	$E_{\pi+\sigma}$ (eV)	$d_{1,0}$ (nm)	$d_{1,1}$ (nm)	d_c (nm)	t_r
NR1	4.8	16.7	0.210	0.117	—	0.04
NR2	4.9	17.9	0.207	0.120	0.36	0.06
NR3	5.6	23.6	0.207	0.122	0.36	0.13
NR4	5.8	24.3	0.203	0.120	0.37	0.34
HOPG	7.0	27.1	0.205	0.119	—	0.45

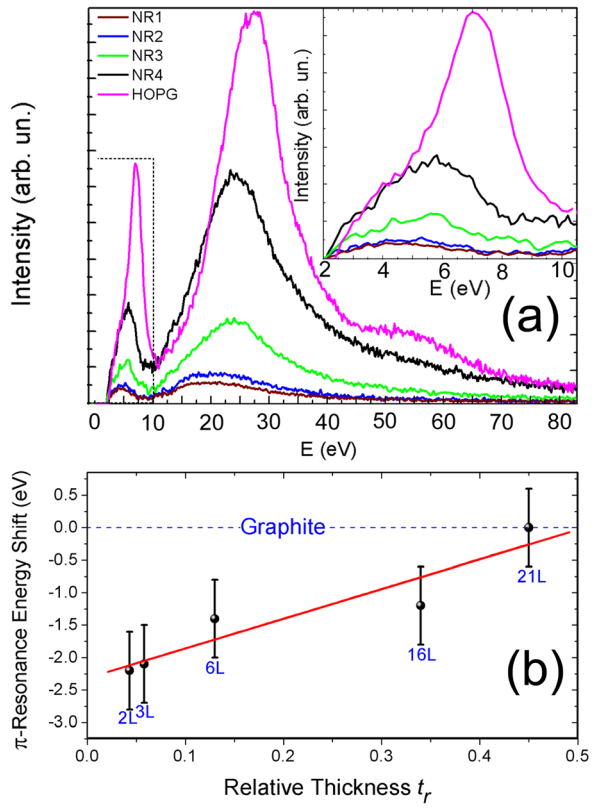

FIG. 3. (Color online) (a) EELS spectra obtained from graphene flakes of different thickness and from graphite. In the inset, the π-resonance peaks are blown up. (b) Energy shift of π-resonance as a function of the relative thickness t_r obtained from the EELS spectra with the log-ratio method. The number of layers (L) reported next to the experimental data points is estimated by calibrating the EELS thickness data to the results of electron diffraction, assuming a linear dependence of t_r on the number of layers.

the case of carbon nanotubes.[21,22] As shown by Eberlein *et al.*,[23] the intensity and the energy position of the surface plasmon losses provide information on the number of graphene layers. In particular, the π- and $\pi+\sigma$-surface plasmons are substantially red-shifted from their values in graphite. Accordingly, for the EELS spectrum *NR1* acquired in region 1 of Fig. 2(a), the resonance peaks, occurring at 7.0 and 27.1 eV in graphite, are shifted to 4.8 and 16.7 eV, respectively (Table I). The position of plasmon modes indicates a double layer, as found with diffraction. Moreover, for the two thinnest spectra, the $\pi+\sigma$-resonance shows a plateau-like shape [Fig. 3(a)], as expected for systems with less than 5 layers.[23] By probing areas of increasing thickness, we observe a continuous shift of the plasmon peaks towards the graphite values and a progressive increase of their intensity. The correlation between the shift and the relative thickness t_r is shown in Fig. 3(b), in which the position of the π-resonance is plotted as a function of t_r.[24] If we assume, in accordance with electron diffraction data, that the thinnest sample is a double layer of graphene the absolute thickness can be estimated by the calibration curve of Fig. 3(b). It is worth noting that conventional analysis, based on EELS data only, would have overestimated t_r in this range of thickness, as it generally occurs for very thin films.[25]

In summary, we have shown that NED and EELS techniques with electron nanometer-sized beams are powerful probes of the local defective structure of graphene. Since defects determine the chemical activity of these systems, the information could be crucial for designing nanoribbons with specific sensitivity and/or surface functionalization.

This work was partially supported by the Queensland Government through the NIRAP project "Solar Powered Nanosensors."

[1]K. S. Novoselov, D. Jiang, F. Schedin, T. J. Booth, V. V. Khotkevich, S. V. Morozov, and A. K. Geim, PNAS **102**, 10451 (2005).
[2]C. Neto, F. Guinea, N. M. R. Peres, K. S. Novoselov, and A. K. Geim, Rev. Mod. Phys. **81**, 109 (2009).
[3]M. Fuhrer, C. Lau, and A. MacDonald, MRS Bull. **35**, 289 (2010).
[4]M. Allen, V. Tung, and R. Kaner, Chem. Rev. **110**, 132 (2010).
[5]M. Terrones, A. Botello-Mendez, J. Campos-Delgado, F. Lopez-Urias, Y. Vega-Cantù, F. Rodriguez-Macias, A. Elias, E. Munoz-Sandoval, A. Cano-Marquez, and J.-C. Charlier, Nanotoday **5**, 351 (2010).
[6]S. Dutta and S. Pati, J. Mater. Chem. **20**, 8207 (2010).
[7]J. Bai and Y. Huang, Mater. Sci. Eng. R. **70**, 341 (2010).
[8]M. Terrones, ACS Nano **4**, 1775 (2010).
[9]J. Meyer, A. K. Geim, M. I. Katsnelson, K. S. Novoselov, T. J. Booth, and S. Roth, Nature **446**, 60 (2007).
[10]U. Bangert, M. H. Gass, A. L. Bleloch, R. R. Nair, and A. K. Geim, Phys. Status Solidi A **206**, 1117 (2009).
[11]A. Fasolino, J. H. Los, and M. I. Katsnelson, Nature Mater. **6**, 858 (2007).
[12]V. B. Shenoy, C. D. Reddy, A. Ramasubramaniam, and Y. W. Zhang, Phys. Rev. Lett. **101**, 245501 (2008).
[13]K. Bets and B. Yakobson, Nano Res. **2**, 161 (2009).
[14]B. V. C. Martins and D. S. Galvao, Nanotechnology **21**, 075710 (2010).
[15]F. Cataldo, G. Compagnini, G. Patanà, O. Ursini, G. Angelini, P. Ribic, G. Margaritondo, A. Cricenti, G. Palleschi, and F. Valentini, Carbon **48**, 2596 (2010).
[16]F. Cataldo, G. Compagnini, L. D'Urso, G. Palleschi, F. Valentini, G. Angelini, and T. Braun, Fullerenes, Nanotubes, Carbon Nanostruct. **18**, 261 (2010).
[17]D. Kosynkin, A. Higginbotham, A. Sinitskii, J. Lomeda, A. Dimiev, K. Price, and J. Tour, Nature **458**, 872 (2009).
[18]M. Diociaiuti, L. Lozzi, M. Passacantando, S. Santucci, P. Picozzi, and M. De Crescenzi, J. Electron Spectrosc. Relat. Phenom. **82**, 1 (1996).
[19]J. M. Zuo, M. Gao, J. Tao, B. Q. Li, R. Twesten, and I. Petrov, Microsc. Res. Tech. **64**, 347 (2004).
[20]We emphasize that the diffraction pattern was recorded from exactly the same area as the HRTEM image in panel (b) and under identical illumination conditions.
[21]O. Stephan, D. Taverna, M. Kociak, K. Suenaga, L. Henrard, and C. Colliex, Phys. Rev. B **66**, 155422 (2002).
[22]P. Castrucci, M. Scarselli, M. De Crescenzi, M. A. El Khakani, and F. Rosei, Nanoscale **2**, 1611 (2010).
[23]T. Eberlein, U. Bangert, R. R. Nair, R. Jones, M. Gass, A. L. Bleloch, K. S. Novoselov, A. Geim, and P. R. Briddon, Phys. Rev. B **77**, 233406 (2008).
[24]The relative thickness of the sample in units of the inelastic mean free path of electrons is obtained from the Poisson statistics of inelastic scattering as $t_r = \log(I/I_0)$, where I_0 is the integrated intensity of the zero-loss peak and I the integral of the whole spectrum.
[25]R. F. Egerton, *Electron Energy-Loss Spectroscopy in the Electron Microscope* (Plenum, New York, 1996).
[26]See supplementary material at http://dx.doi.org/ for SAED spectra.